

## Article

# Electrochemical Characterisation of the Photoanode Containing TiO<sub>2</sub> and SnS<sub>2</sub> in the Presence of Various Pharmaceuticals

Gabrijela Radić<sup>1</sup>, Klara Perović<sup>1</sup>, Tayebah Sharifi<sup>1</sup> , Hrvoje Kušić<sup>1,2</sup>, Marin Kovačić<sup>1</sup>   
and Marijana Kraljić Roković<sup>1,\*</sup> 

<sup>1</sup> Faculty of Chemical Engineering and Technology, University of Zagreb, Marulićev Trg 19, 10000 Zagreb, Croatia

<sup>2</sup> Department for Packaging, Recycling and Environmental Protection, University North, Trg dr. Žarka Dolinara 1, 48000 Koprivnica, Croatia

\* Correspondence: mkralj@fkit.hr

**Abstract:** In this work, the behaviour of photoanodes made of TiO<sub>2</sub>, SnS<sub>2</sub> and TiO<sub>2</sub>/SnS<sub>2</sub> was examined in the presence and absence of pharmaceuticals diclofenac (DCF), memantine hydrochloride (MEM) and salicylic acid (SA). The focus of the current research is on the following photoelectrochemical (PEC) characterisation methods: linear polarisation, electrochemical impedance spectroscopy (EIS), and open circuit potential (OCP) monitoring. Linear polarisation and EIS provided useful information about the interaction between the pharmaceuticals and the photocatalytic materials. The presence of the selected pharmaceuticals affects the OCP value, mainly due to the pH change. The results obtained by PEC characterisation were compared to the photocatalytic (PC) efficiency of pharmaceutical degradation. In addition to the photocurrent response, the linear voltammogram indicates the electrochemical oxidation of DCF and SA. Geometry optimizations using density functional theory (DFT) showed that the HOMO orbitals' position of DCF and SA are above the position of the TiO<sub>2</sub> HOMO level and below the position of the SnS<sub>2</sub> HOMO level. Due to this, the characteristic current peak for DCF and SA was registered, but only for TiO<sub>2</sub> and TiO<sub>2</sub>/SnS<sub>2</sub> photoanodes. The oxidation current peak was not registered for MEM, although *h*<sup>+</sup> scavenging properties were noticed for TiO<sub>2</sub> in the presence of MEM. Apparently, this is an interplay between the protonated and non-protonated forms of MEM and the differences in their HOMO positions.

**Keywords:** photocatalysis; pharmaceuticals adsorption; linear polarisation; electrochemical impedance spectroscopy



**Citation:** Radić, G.; Perović, K.; Sharifi, T.; Kušić, H.; Kovačić, M.; Kraljić Roković, M. Electrochemical Characterisation of the Photoanode Containing TiO<sub>2</sub> and SnS<sub>2</sub> in the Presence of Various Pharmaceuticals. *Catalysts* **2023**, *13*, 909. <https://doi.org/10.3390/catal13050909>

Academic Editors: Hideyuki Katsumata, Giuseppina Iervolino, Huiyao Wang, Jose Luis Vilas Vilela and Leire Ruiz-Rubio

Received: 6 May 2023  
Revised: 16 May 2023  
Accepted: 18 May 2023  
Published: 20 May 2023



**Copyright:** © 2023 by the authors. Licensee MDPI, Basel, Switzerland. This article is an open access article distributed under the terms and conditions of the Creative Commons Attribution (CC BY) license (<https://creativecommons.org/licenses/by/4.0/>).

## 1. Introduction

Photoelectrochemical (PEC) and photocatalytic (PC) processes attract significant attention as promising methods for water remediation and water splitting. Furthermore, PEC effect is fundamental for photocatalytic fuel cells, photocatalytic sensors or for photocatalytic corrosion protection [1–3]. It is therefore not surprising that a large number of papers related to PEC and PC have been published. The development in this field started in 1969 when photoelectrolysis was demonstrated for the first time by *A. Fujishima* and *K. Honda*, who exposed an *n*-type TiO<sub>2</sub> photoanode to UV irradiation resulting in photocurrent and water electrolysis [4].

Their discovery prompted further research in this area using TiO<sub>2</sub> as photoactive material. TiO<sub>2</sub> is attractive due to its high photoresponse, high chemical stability, low cost and nontoxicity. However, it is only active in the ultraviolet (UV) region; therefore, there is a need to develop alternative material with activity in the visible range (Vis) as well, which will enable a more efficient harvesting of solar energy. For this purpose, different approaches, including the dye sensitization of TiO<sub>2</sub> or TiO<sub>2</sub> doping with metals, nitrogen, sulfur or carbon, were developed [4]. TiO<sub>2</sub> application is also hampered by a significant recombination of photogenerated hole–electron (*h*<sup>+</sup> / *e*<sup>−</sup>) pairs; therefore, much attention

has been paid to decreasing its recombination rate. This can be achieved by the non-metal doping of TiO<sub>2</sub> [4], where trapping centers for the photogenerated  $e^-$  are introduced to the TiO<sub>2</sub> structure, or by composite material formation [5,6], where  $h^+/e^-$  pairs are separated by a heterojunction formation. Another approach to increasing solar energy harvesting is the utilization of materials active in the visible spectrum, such as BiVO<sub>4</sub>, SnS<sub>2</sub>, CuS, MoS<sub>2</sub>, or the development of various composite and bilayer structures of these materials.

Pharmaceuticals are known to have a significant impact on the aquatic environment and pose an ecological risk. Accordingly, it is important to develop an innovative and practical water treatment technique, which will be able to effectively remove/degrade such persistent pollutants. The PC or PEC treatments are promising techniques for the degradation of various pharmaceuticals due to their efficiency, simplicity and low cost. These techniques are based on the light absorption by a photoactive material that generates  $h^+/e^-$  pairs. The resulting  $h^+$  reacts with water (i.e., hydroxyl ion (HO<sup>-</sup>)), producing hydroxyl radicals (HO•), as a main representative of reactive oxidation species (ROS), which are involved in the indirect oxidation of pharmaceuticals [7–12]. The photogenerated  $e^-$  in PC reacts with oxygen to form superoxide radicals (O<sub>2</sub>•<sup>-</sup>), while the  $e^-$  generated in PEC is continuously drained to the counter-electrode. The general conclusion for an efficient PEC or PC process is that the adsorption of a pharmaceutical molecule at the surface of a photocatalytic material is highly preferred, enabling the direct oxidation/reduction of pharmaceuticals at the surface, thus overcoming diffusion limit issues related to the transfer of short-lifetime ROS species [13–15]. There are also reports that pharmaceutical oxidation takes place through direct oxidation by the valence band  $h^+$  [8,9,16]. Due to the complexity of the process, the determination of the exact mechanism is a rather challenging task [10,11].

In this work, the influence of three different pharmaceuticals (diclofenac (DCF), me-mantine hydrochloride (MEM), and salicylic acid (SA)), on PEC response and, consequently, PC effectiveness, was studied. Most reports related to DCF PC degradation were carried out using TiO<sub>2</sub> photoactive material [17–20], but there are reports on other materials, such as V<sub>2</sub>O<sub>5</sub> [21], TiO<sub>2</sub>/WO<sub>3</sub> [22–25] or TiO<sub>2</sub>/SnS<sub>2</sub> [5], as well. Silva et al. [26] developed photocatalytic membranes containing TiO<sub>2</sub>. Moctezuma et al. [27] showed that positively charged TiO<sub>2</sub> surface and negatively charged oxygen atoms of the carbonyl group in DCF molecules strongly interact, promoting the quick chemisorption of DCF on the catalyst surface. They also established the relationship between the DCF concentration and the degradation and adsorption rate. Achari et al. [28] demonstrated that the rate of degradation of DCF increases with the increase in concentration up to 25 mg/L of DCF (0.084 mM), which is consistent with pseudo-first-order kinetics. A decrease in the order of reaction is noted with an increase in concentration. Sun et al. [18] studied a PEC process using the I-doped TiO<sub>2</sub> photoanode active in the visible light range; the results revealed that the degradation of DCF was mainly caused by  $h^+$  (66.6%) and HO• (27.6%). In the case of MEM, there are only a few reports, in which TiO<sub>2</sub> and TiO<sub>2</sub>/SnS<sub>2</sub> photocatalysts were used [15,29,30]. Photocatalytic degradation of SA, a widespread water-contaminant, was also reported [31–39]. It was found that the degradation is pH-dependent; an optimal value is found under strong acidic conditions due to the favourable interaction between TiO<sub>2</sub> and SA [33,35]. The strong chemisorption of SA at TiO<sub>2</sub> through the formation of inner sphere surface complexes is a well-known phenomenon. The adsorption takes place through the coordination of deprotonated carboxylates and Ti atoms [32,40–42].

Electrochemical techniques can be a powerful tool in the field of PC or PEC, enabling material and material/solution interface characterisation. A review of the literature has indicated that a large number of reports are related to the photocatalyst characterisation by electrochemical methods; however, reports related to the influence of pharmaceuticals on the photocatalyst electrochemical response are still scarce [11,31,33,35,43,44]. The aim of this work was an examination of the influence of pharmaceuticals (DCF, MEM and SA) on the PEC response of TiO<sub>2</sub>, TiO<sub>2</sub>/SnS<sub>2</sub> and SnS<sub>2</sub> photoactive materials using simple and fast electrochemical methods. For this purpose, linear polarisation, open-circuit potential monitoring and electrochemical impedance spectroscopy were used. This research can

provide a stepping-stone to determine the ideal conditions for PC or PEC treatment. To correlate the results of the PEC characterisation and the PC degradation, DCF and MEM degradation was carried out using TiO<sub>2</sub> or SnS<sub>2</sub> photocatalysts.

## 2. Results and Discussion

In this work, the PEC properties of different materials such as TiO<sub>2</sub>, SnS<sub>2</sub> and TiO<sub>2</sub>/SnS<sub>2</sub> were examined in the presence of three pharmaceuticals (DCF, MEM and SA) and in a pure NaCl solution as benchmark. The structures of the investigated pharmaceuticals are shown as inset figures within Figure 1a–c. The photocurrent density ( $j_{ph}$ ) is the result of the photoactivity of a material, and its value is the difference between light and dark current response ( $j_{ph} = j_{light} - j_{dark}$ ). Therefore, the good PEC activity of TiO<sub>2</sub> in NaCl is evident in Figure 1, as  $j_{light} \gg j_{dark}$ . The dark characteristic for TiO<sub>2</sub> electrodes in NaCl shows no current in the potential range from  $-0.25$  V to 1 V, while the light characteristic shows currents of about  $30 \mu\text{A cm}^{-2}$  (Figure 1a–d). The obtained current values for the illuminated TiO<sub>2</sub> are in agreement with the results of Marugán et al. [45]. As can be seen in Figure 1a–d, by linear polarisation, a constant current value is immediately obtained, which is characteristic of the current saturation of the irradiated electrode. When charge carrier separation in the semiconductor is the performance-limiting step, the current continuously increases with the potential increase, which is not characteristic of our electrode. The fast current saturation was previously associated with the size of the TiO<sub>2</sub> nanoparticles [16,45]. The small TiO<sub>2</sub> P25 particle size used in this work [46] limits the thickness of the depletion layer and prevents complete band-bending through the film, quickly reaching a saturated current density. It is also evident that both dark and light features show a significant current increase at a more positive potential than 1.25 V or more negative potential than  $-0.2$  V (Figure 1a–d), apparently due to the supporting electrolyte reaction [47,48].

It is well-known that, for n-type semiconductors, a depletion layer is present at more positive potentials than the flat-band potential; therefore, no oxidative current is expected in the dark. However, in our experiment, the dark characteristic shows a current peak related to the redox reaction of DCF and SA, with a current peak at  $\sim 1.1$  V (Figure 1a,b) [49]. It is obvious that an electric field above 1 V generates  $h^+$ , enabling the redox reaction of DCF and SA [47]. Similar results were obtained for TiO<sub>2</sub> electrodes in solutions containing antioxidants [50]. The dark characteristic of MEM (Figure 1c) showed no current peak, indicating that, compared to SA and DCF, MEM is more stable during electrochemical oxidation. The presence of pharmaceutical compounds also affected the current value. Again, the influence was similar for DCF and SA solutions (Figure 1a,b) and different for the MEM solution (Figure 1c,d). The responses of irradiated TiO<sub>2</sub> electrodes in DCF and SA solutions show a current peak similar to that of the dark characteristic, as well as a decrease in the current compared to the current in the NaCl solution [35,43]. The decrease in current can be explained by the adsorption of SA and DCF on the electrode surface, blocking the surface-active sites. The literature data have shown that significant amounts of DCF [15] and SA [32,40–42] can be adsorbed on the TiO<sub>2</sub> surface. It is also worth noting that the UV absorption of SA and DCF ( $\lambda_{max,SA} = 240$  nm and  $\lambda_{max,DCF} = 276$  nm) reduces the photon flux available at the TiO<sub>2</sub> surface [35,51], which further reduces the photoactivity of TiO<sub>2</sub>.

A similar linear polarisation response was obtained when the TiO<sub>2</sub> electrode was stabilised in DCF and SA solutions for 5 min or when it was stabilised in the same solution for 30 min before measurement. This observation indicates the fast adsorption process of SA and DCF. On the other hand, the linear polarisation response significantly varied for electrodes stabilised in an MEM solution for 5 min (Figure 1d) and 30 min (Figure 1c). In the short-term stabilisation, the presence of MEM increased the photocurrent. It seems that although MEM could not be oxidised in the dark by an electrochemical process, it is oxidised in the photocatalytic process [15,29]. The current increase indicates the radical/ $h^+$  scavenging properties of MEM, which apparently depend on its concentration (Figure 1d). However, when the electrode is stabilised in the dark for 30 min in the MEM solution, the current decreases, indicating a similar effect to that observed in the case of DCF and SA.

Moreover, it is evident that MEM (Figure 1c) affects the current response to a lesser extent than DCF and SA (Figure 1a,b). This behaviour is expected for MEM due to its structure, which does not absorb UV radiation; it only blocks active sites that are important for the photocatalytic response, while SA and DCF absorb UV radiation.

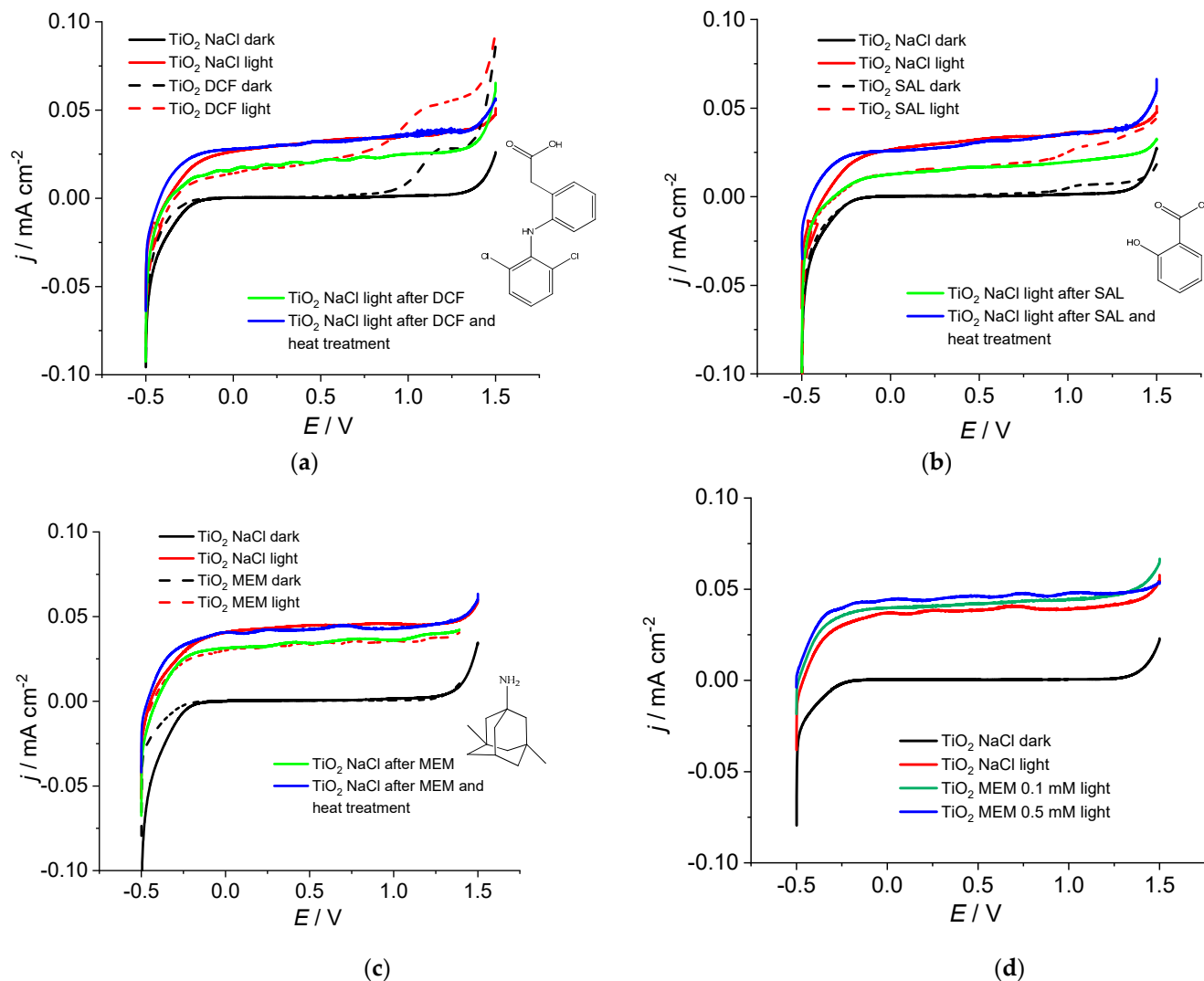


**Figure 1.** Linear sweep voltammetry responses obtained for light and dark characteristics of the  $\text{TiO}_2$  electrode in the presence and absence of (a) DCF, (b) SA, (c,d) MEM. Stabilisation of the electrode in a solution containing DCF, SA or MEM was carried out 30 min before the measurement (a–c). Stabilisation of the electrode in a solution containing MEM was carried out 5 min before measurement (d). The chemical structures of the used pharmaceuticals are shown within the figures (a–c).

To prove that the decrease in current is related to the pharmaceuticals' adsorption, each electrode was thoroughly washed with water after the test and then polarised in NaCl solution (Figure 1a–c). The obtained responses show that the decrease in current is similar to the response obtained in the pharmaceutical solution. It is obvious that the adsorbed pharmaceuticals remain on the electrode surface even after they are transferred to the NaCl solution, so the current decrease is due to the adsorption of pharmaceuticals on the electrode surface. To prove the stability of the  $\text{TiO}_2$  electrode used in this work, each electrode was treated with UV light and annealed in air at  $200^\circ\text{C}$  at the end of the experiment. These procedures completely removed the pharmaceuticals from the electrode surface, and the electrode response in the NaCl solution was the same as before the electrode was exposed

to the pharmaceutical solution (Figure 1a–c). This result doubtlessly supports the previous conclusions regarding current decrease and pharmaceuticals' adsorption.

OCP was recorded to study the generation, accumulation, and recombination of the photoinduced charge carriers in chopped light irradiation (Figure 2a–d). In addition, the influence of pharmaceuticals on the OCP was investigated. When light illumination is applied, the OCP exhibits a more negative value for all samples, which indicates photovoltage value. Although similar behaviour was observed for all tested samples, it is obvious that the most negative value was obtained for the solution containing MEM, while the potential values for solutions containing SA and DCF were less negative compared to the NaCl solution. A similar effect was found in several studies: by Li et al. [31], who investigated the degradation of SA, formic acid and methanol on TiO<sub>2</sub>, by Palmas et al. [48], who investigated the degradation of bisphenol A on TiO<sub>2</sub>, and by Jin et al. [52], who investigated the interactions between methanol and the TiO<sub>2</sub> nanotube assembly. In addition to the influence of pharmaceutical adsorption, pH could also be a determining factor for the electrode potential. In our study, the pH values varied slightly between pH = 5.7 and pH = 6.5. To keep the pH constant in all experiments, additional experiments were performed in buffered solution in the presence and absence of the studied pharmaceuticals (Figure 2b–d). The results obtained in buffered solution (pH = 6) showed that only the presence of MEM slightly affected the OCP value. Therefore, it is obvious that the natural pH changes that occur in the presence of DCF, SA and MEM affect the final OCP value. The effect of adsorption of the studied pharmaceuticals on the OCP value was not significant, suggesting that the addition of pharmaceuticals affects the photocurrent but not the photovoltage.

Figure 3a–c shows the EIS responses of the TiO<sub>2</sub> electrode in NaCl with and without DCF, SA, and MEM. Measurements were performed for the irradiated electrode at the OCP value and at 50 mV, 500 mV, and 1000 mV for DCF, SA, and MEM. The impedance data were analysed using the electrical equivalent circuit, shown as an inset figure within Figure 3a–c. This model provided a reliable description of the electrochemical systems; the numerical values of the impedance parameters for the TiO<sub>2</sub> electrode in NaCl, DCF, SA, and MEM solutions are summarised in Table 1. It is evident that the resistance R1 at the OCP increases with the addition of pharmaceuticals (Figure 3a–c, Table 1a–c), while the value of Q1 for DCF and SA decreases (Table 1a–c). It was concluded that R1 at the OCP is related to the charge transfer resistance (R<sub>ct</sub>) and Q1 is a constant phase element related to the capacitance of the double layer (Q<sub>dl</sub>). A constant phase element is usually introduced instead of an ideal capacitance element because the measured capacitive response is not ideal due to the certain heterogeneity of the electrode surface [53]. Its impedance can be defined by  $Z = [Q(j\omega)n]^{-1}$ , where  $\omega$  is the angular frequency and  $n$  is the power of the constant-phase element. Higher values of the charge transfer resistance in the presence of pharmaceuticals indicate a slower PEC response, which is consistent with the lower current values in the linear voltammogram. It is obvious that the studied pharmaceuticals adsorb on the electrode surface and, in this way, decrease the photoactivity of the electrode. Accordingly, the decrease in capacitance obtained for SA and DCF at OCP can also be explained by the presence of pharmaceutical molecules on the electrode surface. R<sub>ct</sub> was expected to decrease due to the electrode polarisation at more positive potentials than the OCP, due to band-bending and more efficient charge separation. Surprisingly, when polarised from 50 mV to 1 V, the opposite behaviour was observed in both NaCl and pharmaceutical solutions. Therefore, it was concluded that the EIS response obtained for the irradiated electrode at different polarisation potentials (50 mV, 500 mV, and 1000 mV) is related to the space charge properties. This is also supported by the Q1 values, which decrease with increasing potential in agreement with the Mott-Schotky behaviour for the n-type semiconductor [54]. It follows that the Q1 obtained by polarisation at different potentials is related to the space charge capacitance. Although the linear polarisation results indicate that the space charge thickness is confined by the small particle size, it follows from the EIS results that the space charge thickness increases due to electrode polarisation.

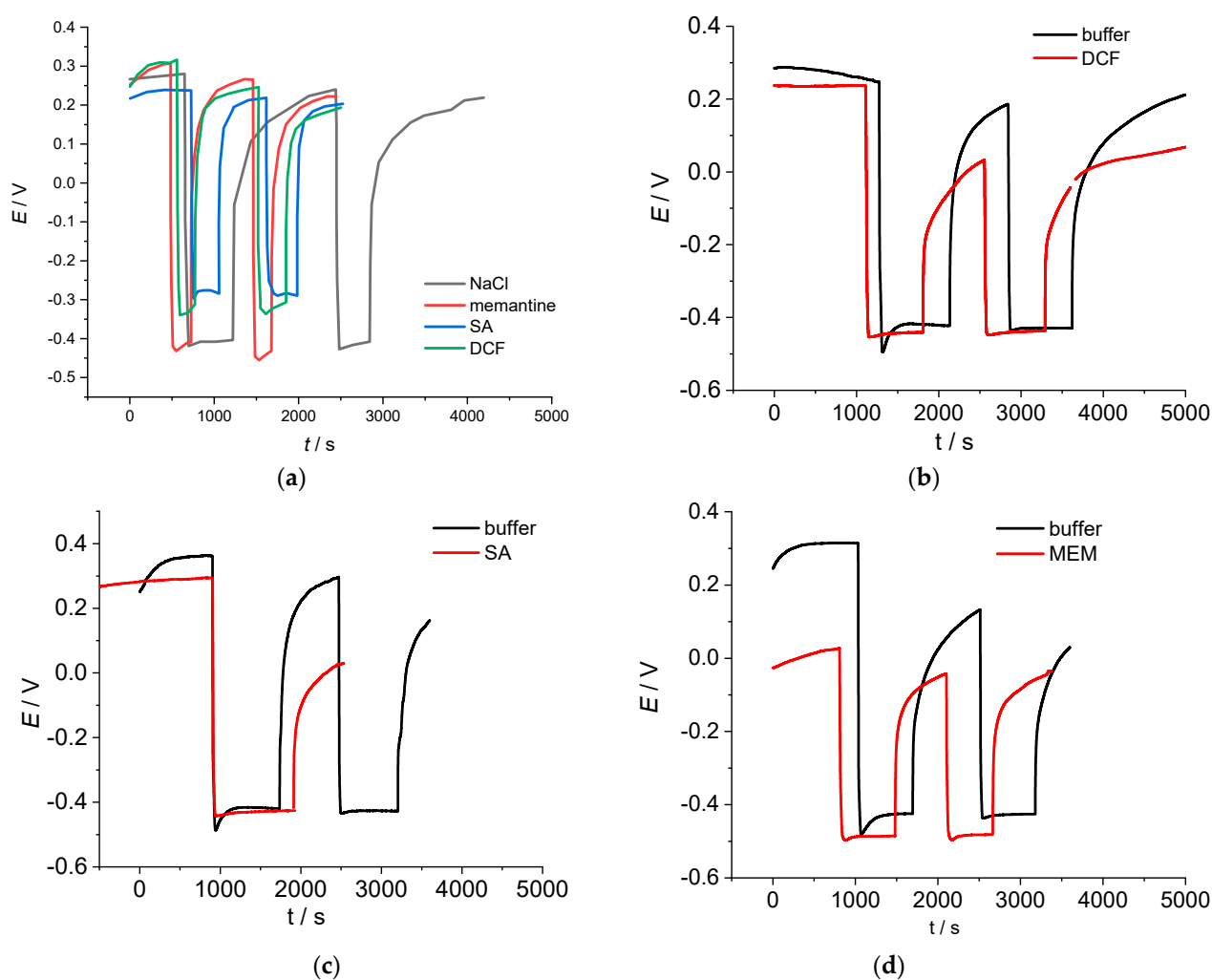


**Figure 2.** Open-circuit potential of the  $\text{TiO}_2$  electrode in chopped light irradiation in (a) NaCl solution containing MEM, SA or DCF, (b) in a buffer solution and a buffer solution containing DCF, (c) in a buffer solution and a buffer solution containing SA, (d) in a buffer solution and a buffer solution containing MEM.

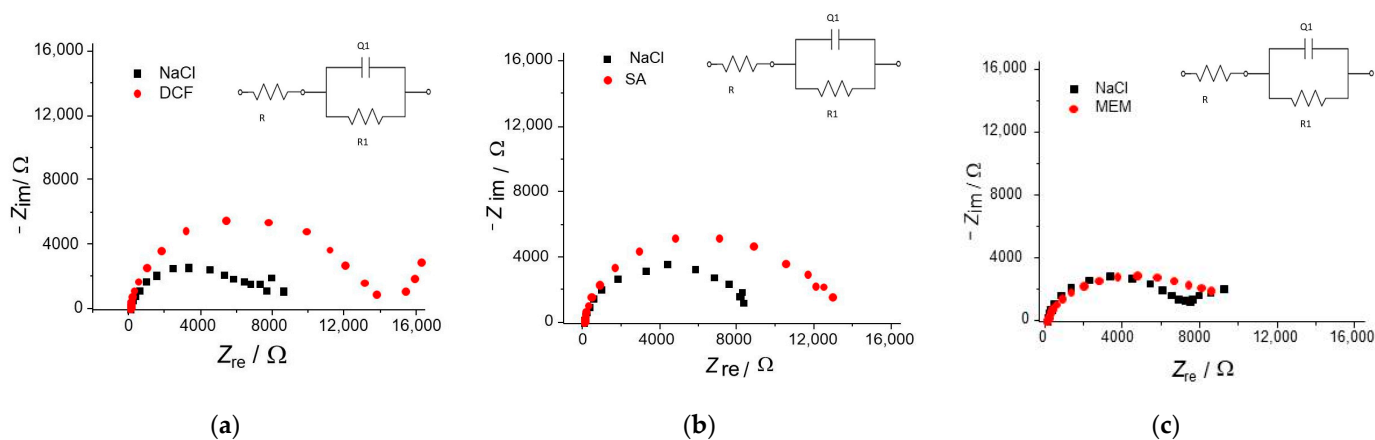


**Figure 3.** The Nyquist plot obtained for the  $\text{TiO}_2$  electrode under UV irradiation at OCP in NaCl solution or NaCl solution containing  $0.1 \text{ mmol dm}^{-3}$  of (a) DCF, (b) SA, and (c) MEM; inset figures present electrical equivalent circuit used to fit the EIS spectra.

**Table 1.** Numerical values of impedance parameters for the TiO<sub>2</sub> electrode in NaCl and (a) DCF, (b) SA and (c) MEM solutions.

<b>(a) for DCF</b>	<b><i>Re</i>/<math>\Omega</math></b>	<b><i>R1</i> <math>\times 10^{-5}/\Omega</math></b>	<b><i>Q1</i> <math>\times 10^5/S s^n</math></b>	<b><i>n1</i></b>
NaCl OCP	54.94	0.069	4.24	0.85
NaCl 50 mV	55.73	1.10	1.48	0.93
NaCl 500 mV	55.34	0.92	1.14	0.94
NaCl 1000 mV	54.42	0.50	1.09	0.92
DCF OCP	57.59	0.13	2.44	0.92
DCF 50 mV	56.82	1.08	1.65	0.92
DCF 500 mV	57.12	0.77	1.23	0.93
DCF 1000 mV	56.69	1.02	1.17	0.92
<b>(b) for SA</b>	<b><i>Re</i>/<math>\Omega</math></b>	<b><i>R1</i> <math>\times 10^{-5}/\Omega</math></b>	<b><i>Q1</i> <math>\times 10^5/S s^n</math></b>	<b><i>n1</i></b>
NaCl OCP	54.44	0.083	2.95	0.91
NaCl 50 mV	56.76	1.13	1.44	0.95
NaCl 500 mV	57.53	1.41	1.14	0.95
NaCl 1000 mV	56.88	2.19	0.967	0.95
SA OCP	53.75	1.22	2.65	0.92
SA 50 mV	57.44	0.731	1.57	0.95
SA 500 mV	54.28	1.17	1.18	0.95
SA 1000 mV	53.90	1.18	1.21	0.95
<b>(c) for MEM</b>	<b><i>Re</i>/<math>\Omega</math></b>	<b><i>R1</i> <math>\times 10^{-5}/\Omega</math></b>	<b><i>Q1</i> <math>\times 10^5/S s^n</math></b>	<b><i>n1</i></b>
NaCl OCP	56.18	0.068	2.02	0.92
NaCl 50 mV	55.63	0.973	0.724	0.94
NaCl 500 mV	54.41	2.545	1.29	0.94
NaCl 1000 mV	53.98	2.275	0.516	0.96
MEM OCP	51.22	0.070	2.20	0.92
MEM 50 mV	51.54	1.250	2.11	0.92
MEM 500 mV	51.22	1.208	0.84	0.94
MEM 1000 mV	51.30	1.628	0.38	0.95

From the presented results, it can be concluded that photoelectrochemical measurements are a simple and fast method to determine the adsorption process, as well as the influence of pharmaceuticals on the response of the photoactive material. Therefore, additional measurements were performed with SnS<sub>2</sub> and TiO<sub>2</sub>/SnS<sub>2</sub> electrodes. Due to its small band gap, SnS<sub>2</sub> can be used for solar radiation utilisation, so its PEC study is of great importance. SnS<sub>2</sub> is also an attractive material for hydrogen production because the position of its conduction band is more negative than the standard reduction potential of H<sub>2</sub>O/H<sub>2</sub>. In PEC processes, the  $h^+$  generated by SnS<sub>2</sub> is suitable for oxygen generation but not for HO• generation; the potential of its valence band does not allow for such a reaction. However, TiO<sub>2</sub>/SnS<sub>2</sub> has been used in PC processes as a photoactive material for the degradation of pharmaceutical compounds because it forms strong radicals with the help of excited electrons [5]. The information obtained from the PEC study may be useful for the application of this material in the PC degradation of pharmaceuticals and, furthermore, for the application of this material in hydrogen production.

From Figure 4, it is evident that  $j_{\text{light}} \gg j_{\text{dark}}$ , indicating the good photoactivity of the TiO<sub>2</sub>/SnS<sub>2</sub> composite material. The current response of the TiO<sub>2</sub>/SnS<sub>2</sub> electrode in the NaCl solution is not constant, as in the case of TiO<sub>2</sub>. During the potential sweep, the current

value increases continuously, which is a consequence of the more effective separation of the photogenerated charge carriers in the presence of an electric field. The more effective charge separation is the result of a process involving an upward bending of the conduction and valence bands and the formation of a depletion layer at the electrode/electrolyte surface, which directs the photogenerated  $e^-$  to the FTO substrate and  $h^+$  to the electrode/electrolyte interface. This phenomenon is related to the influence of the positive potential on the  $n$ -type semiconductors [47,54]. A thicker depletion layer is expected for SnS<sub>2</sub> compared to TiO<sub>2</sub> because of the larger SnS<sub>2</sub> particle size. The morphological properties of SnS<sub>2</sub> and TiO<sub>2</sub>/SnS<sub>2</sub> were reported by Kovacic et al. [55]. The presence of pharmaceuticals reduces the TiO<sub>2</sub>/SnS<sub>2</sub> current in the NaCl solution (Figure 4) in a similar way as in the case of TiO<sub>2</sub> (Figure 1a–c). For DCF and SA solutions, the current decrease is evident only at potentials more negative than 0.5 V, because the current peak associated with the electrochemical reaction dominates at positive potentials higher than 0.5 V (Figure 4a,b). Although SA and DCF do not absorb light in the visible range, they affect the photocurrent response by blocking the active sites for the photocatalytic reaction. In the case of MEM (Figure 4c), a significant current decrease was obtained, which is different from the behaviour of TiO<sub>2</sub> in the MEM solution (Figure 1c). These results indicate that MEM affects the composite much more than TiO<sub>2</sub>.

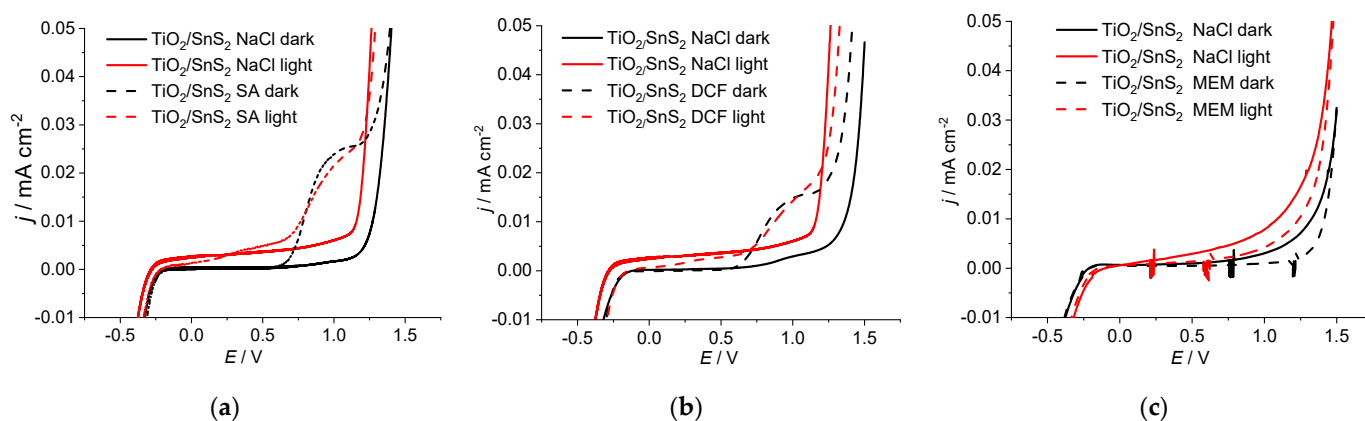


**Figure 4.** Linear sweep voltammetry photocurrent response of the TiO<sub>2</sub>/SnS<sub>2</sub> electrode in the presence and absence of (a) SA, (b) DCF and (c) MEM.

To clarify the obtained behaviour, the SnS<sub>2</sub> electrode was also investigated in the presence of the studied pharmaceuticals. The results (Figure 5) indicate that the SnS<sub>2</sub> electrode has a higher photocurrent compared to the TiO<sub>2</sub>/SnS<sub>2</sub> electrode (Figure 4), which is not surprising since SnS<sub>2</sub> has a smaller band gap compared to TiO<sub>2</sub> and absorbs light in the visible region, while TiO<sub>2</sub> is not active in the visible region. It should be noted that the LED illumination used in this work provides only visible light [56]. The current value in the NaCl solution for SnS<sub>2</sub> and TiO<sub>2</sub>/SnS<sub>2</sub> electrodes at 0.5 V was about 6  $\mu$ A and 4  $\mu$ A, respectively, while at 1 V it was 12  $\mu$ A and 6  $\mu$ A, respectively. The influence of SA and DCF on the electrochemical response of SnS<sub>2</sub> electrode (Figure 5a,b) was not significant; however, the influence of MEM (Figure 5c) was similar to that in the case of TiO<sub>2</sub>/SnS<sub>2</sub>. It is also evident from Figure 5 that the characteristic current peak related to the redox reaction of DCF and SA did not occur for the SnS<sub>2</sub> electrode, while it did for TiO<sub>2</sub> and TiO<sub>2</sub>/SnS<sub>2</sub>. This can be explained by the position of the valence band of SnS<sub>2</sub>, which is above the Fermi levels of SA and DCF. The current peak was obtained for the TiO<sub>2</sub>/SnS<sub>2</sub> composite electrode due to the position of the TiO<sub>2</sub> valence band.

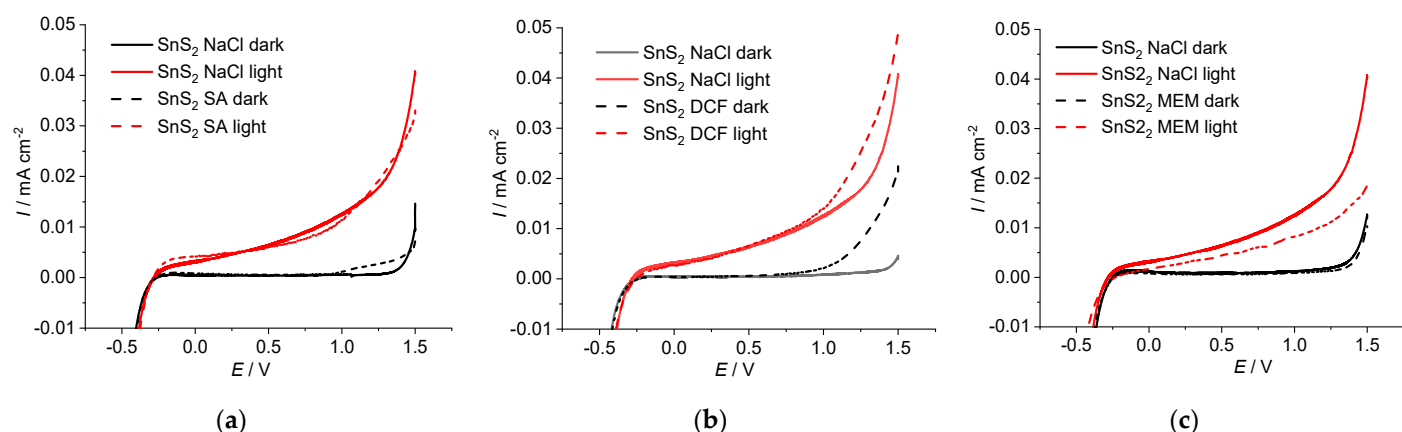


**Figure 5.** Linear sweep voltammetry photocurrent response of the SnS<sub>2</sub> electrode in the presence and absence of (a) SA, (b) DCF and (c) MEM.

To confirm this, DFT calculations were performed for DCF, MEM and SA. The oxidation of pharmaceuticals in the presence of SnS<sub>2</sub> and TiO<sub>2</sub> depends on the HOMO position of the pharmaceuticals and the HOMO position of SnS<sub>2</sub> and TiO<sub>2</sub>. The position of HOMO of the metal oxide used in this work was described in a previous work [5], and in this work it is related to the HOMO positions of the studied pharmaceuticals (Figure 6, Table 2).

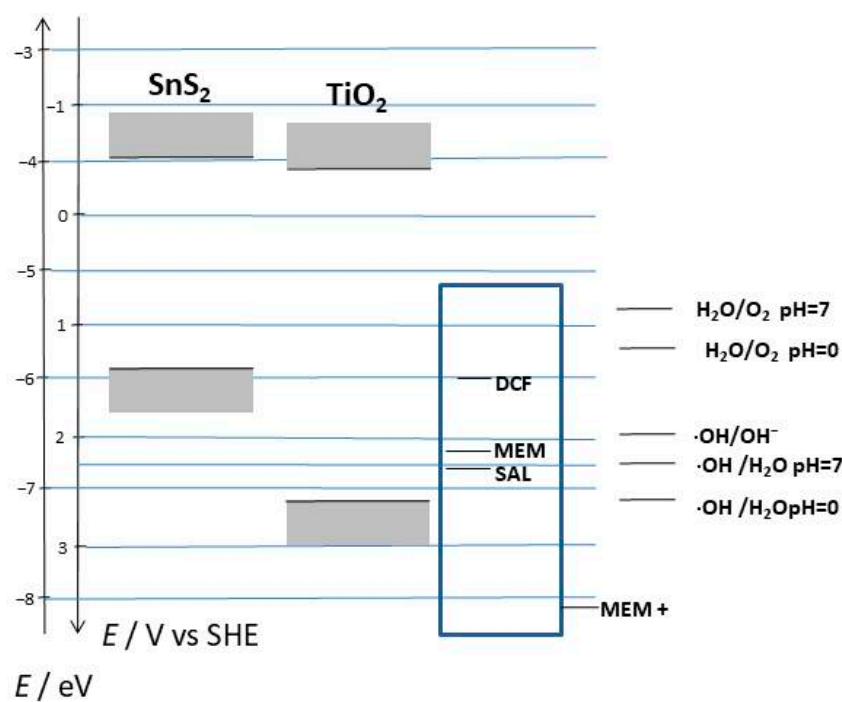


**Figure 6.** Energy-band diagram of TiO<sub>2</sub> and SnS<sub>2</sub> [5], together with the thermodynamic data of possible water and pharmaceutical redox reactions at the metal oxide/electrolyte interphase.

**Table 2.** Quantum chemical reactivity descriptors obtained from HOMO and LUMO energies for DCF, MEM, SA and their charged forms by DFT calculations.

	DCF	DCF <sup>-</sup>	SA	SA <sup>-</sup>	MEM	MEM <sup>+</sup>
$E_{\text{HOMO}}$ , eV	-6.044	-5.615	-6.772	-6.073	-6.684	-8.102
$E_{\text{LUMO}}$ , eV	-1.084	-0.980	-1.790	-0.896	-0.083	-0.448
$\Delta E_{\text{HOMO-LUMO}}$ , eV	-4.960	-4.636	-4.982	-5.177	-6.601	-7.654

It follows that the HOMO position of SA and DCF is above the position of TiO<sub>2</sub>, leading to the oxidation of SA and DCF by the electrochemically generated  $h^+$ . This is well-supported by the current peak formed during electrochemical polarisation (Figure 1a,b). The HOMO position of MEM strongly depends on its protonation. The  $h^+$ -scavenging effect of MEM (Figure 1c) indicates that the unprotonated form was involved in the PEC reaction. It is obvious that the protonated form of MEM (MEM<sup>+</sup>) with the position of HOMO below that of TiO<sub>2</sub> is important for electrochemical oxidation at high potentials. The unfavourable ratio between the TiO<sub>2</sub> HOMO and the MEM<sup>+</sup> HOMO prevents the electrochemical oxidation of MEM<sup>+</sup> and the formation of current peaks (Figure 1c). For the SnS<sub>2</sub> electrode, the situation is completely different because  $h^+$  cannot oxidise SA, DCF, or MEM, resulting in no current peak occurring when the SnS<sub>2</sub> electrode is polarised.

Finally, considering the results obtained for TiO<sub>2</sub>, TiO<sub>2</sub>/SnS<sub>2</sub> and SnS<sub>2</sub> electrodes, it can be concluded that the adsorption of SA and DCF was most pronounced at the TiO<sub>2</sub> electrode (Figure 1a,b), while MEM adsorption occurred at the SnS<sub>2</sub> electrode (Figures 4c and 5c). This behaviour is supported by the pK<sub>a</sub> values for DCF, SA and MEM, as well as by the pH values of solutions, which are 4.15 (pH = 5.9), 3 (pH = 5.7) and 10.5 (pH = 6.45), respectively, and by the point of zero charge (pH<sub>PZC</sub>) values of TiO<sub>2</sub> and SnS<sub>2</sub>, which are 6 and 4.61, respectively [5]. Negatively charged DCF and SA are more strongly adsorbed on nearly neutral TiO<sub>2</sub> than on negatively charged SnS<sub>2</sub>, while positively charged MEM is more strongly adsorbed on negatively charged SnS<sub>2</sub> than on nearly neutral TiO<sub>2</sub>.

Considering the negative correlation between adsorption and photocurrent behaviour, it follows that UV irradiation and photoactive material TiO<sub>2</sub> are suitable for the photocatalytic degradation of MEM, while visible light and photoactive material SnS<sub>2</sub> are more suitable for the degradation of SA and DCF. The radical/ $h^+$ -scavenging effect of MEM contributes to a higher photocurrent, resulting in a more effective degradation of the pharmaceutical pollutants. The TiO<sub>2</sub> photocurrent registered in the presence of MEM (43  $\mu$ A) is 9.77 times higher than that of SnS<sub>2</sub> (4.4  $\mu$ A) in the same solution. However, in the case of SA and DCF, the degradation by visible light and the photoactive material SnS<sub>2</sub> is more acceptable. The higher photocurrents, as well as a lower pharmaceutical influence, give SnS<sub>2</sub> preference over the TiO<sub>2</sub>/SnS<sub>2</sub> electrode. Although the SnS<sub>2</sub> photocurrent in the presence of DCF and SA (6.3  $\mu$ A and 6.8  $\mu$ A) is lower than the TiO<sub>2</sub> photocurrent in the same solution (17.0  $\mu$ A and 20.0  $\mu$ A), the ratio is 2.72 (Table 3) for DCF and 2.94 for SA. Thus, it is obvious that the ratio is not as large as in the case of MEM and TiO<sub>2</sub>.

**Table 3.** Comparison of the results obtained by the PEC characterisation, current density at 0.5 V (Figure 1a,c and Figure 5b,c), and results obtained by PC process (TiO<sub>2</sub> and SnS<sub>2</sub> degradation efficiency for DCF and MEM).

	Catalyst	PEC $j_{0.5V}/\mu A$	$j_{TiO_2,0.5V}/j_{SnS_2,0.5V}$	Degradation Efficiency/%	TiO <sub>2</sub> PC Efficiency/SnS <sub>2</sub> PC Efficiency
DCF	TiO <sub>2</sub>	17	2.70	79.86	1.34
	SnS <sub>2</sub>	6.3		58.75	
MEM	TiO <sub>2</sub>	43	9.77	80.70	4.15
	SnS <sub>2</sub>	4.4		19.43	

To correlate the PEC results with the PC process, the degradation of DCF and MEM was carried out using TiO<sub>2</sub> and UV light and SnS<sub>2</sub> and LED irradiation. From Table 3, it can be seen that the DCF degradation ratio is 1.34 times higher in the case of TiO<sub>2</sub>, and the MEM degradation ratio is 4.15 times higher in the case of TiO<sub>2</sub> than SnS<sub>2</sub>. Although the ratio of  $j_{TiO_2, 0.5 V} / j_{SnS_2, 0.5 V}$  does not correspond to the (TiO<sub>2</sub> PC efficiency)/(SnS<sub>2</sub> PC efficiency) (Table 3), it has been shown in this work that electrochemical methods can provide useful and fast information about the photocatalytic degradation of a pharmaceutical. Moreover, the photoactivity of the anode affects the overall current within the electrochemical system; therefore, this aspect is also important for the hydrogen production process [57].

### 3. Materials and Methods

#### 3.1. Photocatalyst Synthesis and Immobilization

The TiO<sub>2</sub> used in this work was Aeroxide P25 TiO<sub>2</sub> (TiO<sub>2</sub>-P25, Evonik). The hydrothermal method, according to a procedure adopted from Zhang et al. [58], was applied to prepare SnS<sub>2</sub> and TiO<sub>2</sub>/SnS<sub>2</sub> composite. Hence, SnS<sub>2</sub> was synthesized by dissolving an aliquot of tin(IV) chloride and thioacetamide precursor in a 5% *v/v* solution of acetic acid in ethanol with constant stirring in a Teflon reaction vessel, which was then transferred to a stainless steel autoclave and treated for 12 h at 180 °C. After cooling naturally to room temperature, the obtained suspension was rinsed with distilled water, centrifuged (3500 rpm for 3 min), dried in a vacuum (3 h at 60 °C), and then homogenized with a porcelain pestle and mortar. The same procedure was applied for TiO<sub>2</sub>/SnS<sub>2</sub> composite synthesis, using corresponding precursors (tin(IV) chloride, thioacetamide, and TBO); the stoichiometric was adjusted to obtain a composite with a SnS<sub>2</sub> content of 40%.

In order to prepare the working electrodes (TiO<sub>2</sub> electrode, SnS<sub>2</sub> electrode and TiO<sub>2</sub>/SnS<sub>2</sub> electrode) for PEC measurements, spin-coating (KW-4A spin-coater, Chemat Technology, Northridge, CA 91324, USA) was performed at 1500 rpm to immobilize the photoactive materials (TiO<sub>2</sub>, SnS<sub>2</sub> or TiO<sub>2</sub>/SnS<sub>2</sub>) onto FTO glass slides. Prior to the coating, FTO glass slides were sonicated for 10 min separately in acetone, ethanol, and Milli Q water, and then dried at room temperature. Then, for each layer, 100 µL aliquot of photoactive material dispersed within the titania/silica binder [56] was dropped onto the FTO substrate and dried at 200 °C for 2 h in a laboratory oven (UN-55, Memmert, Schwabach, Germany).

It should be noted that the characterisation of the prepared materials (SnS<sub>2</sub> and TiO<sub>2</sub>/SnS<sub>2</sub>) for their morphological, structural, surface and optical properties was reported in our previous publications [5,55].

#### 3.2. Photoelectrochemical Characterisation

PEC measurements of the as-prepared materials were performed using a potentiostat/galvanostat (SP-150, Biologic, Seyssinet-Pariset, France) and a three-electrode system, consisting of a Pt counter-electrode, SCE reference electrode, and as-prepared photoactive materials (TiO<sub>2</sub>, SnS<sub>2</sub> or TiO<sub>2</sub>/SnS<sub>2</sub>) working electrode (1 cm<sup>2</sup>). For the TiO<sub>2</sub> electrode, a UV-A light source was used, while for SnS<sub>2</sub> or TiO<sub>2</sub>/SnS<sub>2</sub> electrodes, an LED light source was used [56].

Investigations were performed in 0.1 mol dm<sup>-3</sup> NaCl solution in the presence and absence of 0.1 mmol dm<sup>-3</sup> of the studied pharmaceuticals (DCF, SA or MEM). Additional measurements were carried out in the presence of MEM with a concentration of 0.5 mmol dm<sup>-3</sup>. Linear sweep voltammetry was carried out with a scan rate of 20 mV s<sup>-1</sup> in the dark and under light illumination. All potentials are reported versus saturated calomel electrode (SCE).

Electrochemical impedance spectroscopy (EIS) measurements were carried out for the TiO<sub>2</sub> electrode in the three-electrode system in 0.1 mol dm<sup>-3</sup> NaCl solution, and in the presence and absence of 0.1 mmol dm<sup>-3</sup> of studied pharmaceuticals (DCF, SA or MEM). The frequency range was scanned from 100 kHz to 100 mHz at OCP and a dc potential of 0 V, 0.5 V and 1 V vs. SCE, with the amplitude of ±5 mV. The impedance spectra were analysed by complex non-linear least squares regression with modulus weighting using ZSimpWin 3.2 software.

#### 3.3. Photocatalytic Degradation Experiments

Photocatalytic degradation experiments were performed for DCF and MEM using TiO<sub>2</sub> and SnS<sub>2</sub> photocatalysts for each pharmaceutical compound. Degradation was carried out in a glass reactor using 100 mL of 1 mg mL<sup>-1</sup> pharmaceutical solution and 0.1 g of the powdered photocatalytic material. The experiments were carried out for 2 h under continuous stirring, including 30 min in dark conditions and 90 min under light illumination. For TiO<sub>2</sub> photoactive material, a UV-A light source was used, and for SnS<sub>2</sub>, an LED light source was used.

The changes in concentration of selected pharmaceuticals DCF and MEM during applied PC treatment were monitored by LC-20 series (Shimadzu, Kyoto, Japan) HPLC equipped with an SPD-M20A UV/DAD detector (Shimadzu, Kyoto, Japan). It should be noted that MEM detection was performed, employing a pre-column derivatization procedure, explained in detail in our previous paper [15]. For the detection of derivated MEM products on the HPLC instrument, a gradient elution method, was used with an initial methanol (HPLC grade, Darmstadt, Sigma-Aldrich, St. Louis, MO, USA) concentration of 85%, which was increased during the course of detection up to 95% *v/v*; maximum detection peak was  $\lambda = 265$  nm. DCF samples were analyzed using an isocratic chromatographic method, with a mobile phase made of 70% *v/v* methanol and 30% 0.1 mM aqueous formic acid (HPLC grade, Sigma-Aldrich); maximum detection peak was  $\lambda = 276$  nm. In both cases, a Zorbax Eclipse C18 (Agilent, Santa Clara, CA 95051, USA), 250 mm  $\times$  4.6 mm (5  $\mu$ m) column was used.

### 3.4. Computational Details

Geometry optimizations using density functional theory (DFT) of DCF, SA, and MEM in aqueous medium were performed in Gaussian16 rev. C [59]. For this purpose, the B3LYP hybrid functional based on Becke's three-parameter hybrid function (B3) and combined with Lee–Yang–Parr (LYP) correlation hybrid functional [60–63] was used with the 6-311+G(2d,2p) basis set [64]. The polarizable continuum model (PCM) using the integral equation formalism variant (IEFPCM), as implemented in Gaussian, was used to simulate the effect of the solvent [65,66]. Tight convergence criteria were used for both the SCF and optimization convergence, along with a "superfine" integration grid. The obtained structures were confirmed to be minimal by frequency calculations, indicating that the obtained structures are stationary points.

## 4. Conclusions

In this work, PEC characterisation demonstrated a notable effect of the adsorption of DCF, SA, and MEM on various photocatalysts via linear polarisation and electrochemical impedance spectroscopy measurements. On the other hand, the OCP values were only somewhat affected by the presence of pharmaceuticals, mainly due to the pH change. The adsorption resulted in a decrease in photocurrents and an increase in the charge transfer resistance. The significant decrease in the TiO<sub>2</sub> photocurrent was achieved in the presence of DCF and SA. Furthermore, an increase in TiO<sub>2</sub> photocurrent was obtained in a solution containing MEM, indicating the positive effect of MEM on the photocurrent value. It is important to point out that this effect was only observed when TiO<sub>2</sub> was stabilised for a short time in the MEM solution. When illuminated with visible light, higher photocurrent values were obtained for SnS<sub>2</sub> compared to TiO<sub>2</sub>/SnS<sub>2</sub>. The decrease in the photocurrent observed for TiO<sub>2</sub>/SnS<sub>2</sub> and SnS<sub>2</sub> was more pronounced for MEM than for SA and DCF, indicating a strong interaction between MEM and SnS<sub>2</sub>. The weaker interaction of SA and DCF with SnS<sub>2</sub> compared to TiO<sub>2</sub> does not significantly reduce the photocurrent, especially in the case of SnS<sub>2</sub>. The obtained results indicate that TiO<sub>2</sub> is suitable for the photocatalytic degradation of MEM, while SnS<sub>2</sub> is suitable for the degradation of SA and DCF. The results obtained by PEC characterisation can be related to the PC efficiency.

**Author Contributions:** Conceptualization, M.K.R.; methodology, M.K.R. and T.S.; software, M.K.; investigation, G.R. and K.P.; resources, H.K.; data curation, G.R.; writing—original draft preparation, M.K.R. and G.R.; writing—review and editing, M.K.R., H.K. and T.S.; supervision, M.K.R.; funding acquisition, H.K. All authors have read and agreed to the published version of the manuscript.

**Funding:** This research was funded by Croatian Science Foundation, grant number IP-2018-01-1982 Croatian Government and the European Union through the European Regional Development Fund, grant number KK.01.1.1.04.0001.

**Data Availability Statement:** The data presented in this study are available on request from the corresponding author.

**Acknowledgments:** We would like to acknowledge the financial support through project financed by Croatian Science Foundation (Nano-sized Solar-active Catalysts for Environmental Technologies, IP-2018-01-1982) and project financed by Croatian Government and the European Union through the European Regional Development Fund (Water Purification and Energy Conversion using Novel Composite Materials and Solar Irradiation, KK.01.1.1.04.0001).

**Conflicts of Interest:** The authors declare no conflict of interest. The funders had no role in the design of the study; in the collection, analyses, or interpretation of data; in the writing of the manuscript; or in the decision to publish the results.

## References

1. Albistur, A.; Rivero, P.J.; Esparza, J.; Rodríguez, R. Evaluation of the Photocatalytic Activity and Anticorrosion Performance of Electrospun Fibers Doped with Metallic Oxides. *Polymers* **2021**, *13*, 2011. [[CrossRef](#)] [[PubMed](#)]
2. He, Y.; Chen, K.; Leung, M.K.H.; Zhang, Y.; Li, L.; Li, G.; Xuan, J.; Li, J. Photocatalytic fuel cell—A review. *Chem. Eng. J.* **2022**, *428*, 131074. [[CrossRef](#)]
3. Sun, X.; Wang, C.; Su, D.; Wang, G.; Zhong, Y. Application of Photocatalytic Materials in Sensors. *Adv. Mater. Technol.* **2020**, *5*, 1900993. [[CrossRef](#)]
4. Basavarajappa, P.S.; Patil, S.B.; Ganganagappa, N.; Reddy, K.R.; Raghu, A.V.; Reddy, C.V. Recent progress in metal-doped TiO<sub>2</sub>, non-metal doped/codoped TiO<sub>2</sub> and TiO<sub>2</sub> nanostructured hybrids for enhanced photocatalysis. *Int. J. Hydrogen Energy* **2020**, *45*, 7764–7778. [[CrossRef](#)]
5. Kovacic, M.; Katic, J.; Kusic, H.; Loncaric Bozic, A.; Metikos Hukovic, M. Elucidating the photocatalytic behavior of TiO<sub>2</sub>-SnS<sub>2</sub> composites based on their energy band structure. *Materials* **2018**, *11*, 1041. [[CrossRef](#)] [[PubMed](#)]
6. Perovic, K.; dela Rosa, F.; Kovacic, M.; Kusic, H.; Lavrencic Stangar, U.; Fresno, F.; Dionysiou, D.D.; Loncaric Bozic, A. Recent achievements in development of TiO<sub>2</sub>-based composite photocatalytic materials for solar driven water purification and splitting. *Materials* **2020**, *13*, 1338. [[CrossRef](#)] [[PubMed](#)]
7. Sambur, J.B.; Chen, P. Distinguishing Direct and Indirect Photoelectrocatalytic Oxidation Mechanisms Using Quantitative Single-Molecule Reaction Imaging and Photocurrent Measurements. *J. Phys. Chem. C* **2016**, *120*, 20668–20676. [[CrossRef](#)]
8. Mena, E.; Rey, A.; Beltrán, F.J. TiO<sub>2</sub> photocatalytic oxidation of a mixture of emerging contaminants: A kinetic study independent of radiation absorption based on the direct-indirect model. *Chem. Eng. J.* **2018**, *339*, 369–380. [[CrossRef](#)]
9. Villarreal, T.L.; Gómez, R.; Gonzalez, M.; Salvador, P. A Kinetic Model for Distinguishing between Direct and Indirect Interfacial Hole Transfer in the Heterogeneous Photooxidation of Dissolved Organics on TiO<sub>2</sub> Nanoparticle Suspensions. *J. Phys. Chem. B* **2004**, *108*, 20278–20290. [[CrossRef](#)]
10. Schneider, J.T.; Firak, D.S.; Ribeiro, R.R.; Peralta-Zamora, P. Use of scavenger agents in heterogeneous photocatalysis: Truths, half-truths, and misinterpretations. *Phys. Chem. Chem. Phys.* **2020**, *22*, 15723–15733. [[CrossRef](#)]
11. Villarreal, T.L.; Gómez, R.; Neumann-Spallart, M.; Alonso-Vante, N.; Salvador, P. Semiconductor Photooxidation of Pollutants Dissolved in Water: A Kinetic Model for Distinguishing between Direct and Indirect Interfacial Hole Transfer. I. Photoelectrochemical Experiments with Polycrystalline Anatase Electrodes under Current Doubling and Absence of Recombination. *J. Phys. Chem. B* **2004**, *108*, 15172–15181. [[CrossRef](#)]
12. Yalavarthi, R.; Zboril, R.; Schmuki, P.; Naldoni, A.; Kment, S. Elucidating the role of surface states of BiVO<sub>4</sub> with Mo doping and a CoOOH co-catalyst for photoelectrochemical water splitting. *J. Power Sources* **2021**, *483*, 229080. [[CrossRef](#)]
13. Levchuk, I.; Sillanpää, M. Titanium dioxide—Based nanomaterials for photocatalytic water treatment. In *Advanced Water Treatment*; Sillanpää, M., Ed.; Elsevier: Amsterdam, The Netherlands, 2020; pp. 1–56. ISBN 978-0-12-819225-2. [[CrossRef](#)]
14. Gilja, V.; Novaković, K.; Travas-Sejdic, J.; Hrnjak-Murgić, Z.; Kraljić Roković, M.; Žic, M. Stability and Synergistic Effect of Polyaniline/TiO<sub>2</sub> Photocatalysts in degradation of Azo Dye in Wastewater. *Nanomaterials* **2017**, *7*, 412. [[CrossRef](#)] [[PubMed](#)]
15. Kovacic, M.; Papac, J.; Kusic, H.; Karamanis, P.; Loncaric Bozic, A. Degradation of polar and non-polar pharmaceutical pollutants in water by solar assisted photocatalysis using hydrothermal TiO<sub>2</sub>-SnS<sub>2</sub>. *Chem. Eng. J.* **2020**, *382*, 122826. [[CrossRef](#)]
16. Monllor-Satoca, D.; Bonete, P.; Djellabi, R.; Cerrato, G.; Operti, L.; Gómez, R.; Bianchi, C.L. Comparative Photo-Electrochemical and Photocatalytic Studies with Nanosized TiO<sub>2</sub> Photocatalysts towards Organic Pollutants Oxidation. *Catalysts* **2021**, *11*, 349. [[CrossRef](#)]
17. Cui, Y.; Deng, X.; Ma, Q.; Zhang, H.; Cheng, X.; Li, X.; Xie, M.; Cheng, Q.; Li, B. Kinetics of photoelectrocatalytic degradation of diclofenac using n, s Co-doped TiO<sub>2</sub> nano-crystallite decorated TiO<sub>2</sub> nanotube arrays photoelectrode. *Environ. Prot. Eng.* **2018**, *44*, 117–130. [[CrossRef](#)]
18. Liu, D.; Wang, J.; Zhou, J.; Xi, Q.; Li, X.; Nie, E.; Piao, X.; Sun, Z. Fabricating I doped TiO<sub>2</sub> photoelectrode for the degradation of diclofenac: Performance and mechanism study. *Chem. Eng. J.* **2019**, *396*, 968–978. [[CrossRef](#)]
19. Hey, G.; Vega, S.R.; Fick, J.; Tysklind, M.; Ledin, A.; la Cour Jansen, J.; Andersen, H.R. Removal of pharmaceuticals in WWTP effluents by ozone and hydrogen peroxide. *Water SA* **2014**, *40*, 165–174. [[CrossRef](#)]
20. Cheng, X.; Cheng, Q.; Li, B.; Deng, X.; Li, J.; Wang, P.; Zhang, B.; Liuc, H.; Wang, X. One-step construction of N/Ti<sup>3+</sup> codoped TiO<sub>2</sub> nanotubes photoelectrode with high photoelectrochemical and photoelectrocatalytic performance. *Electrochim. Acta* **2015**, *186*, 442–448. [[CrossRef](#)]

21. Oliveros, A.N.; Pimentel, J.A.I.; de Luna, M.D.G.; Garcia-Segura, S.; Abarca, R.R.M.; Doong, R. Visible-light photocatalytic diclofenac removal by tunable vanadium pentoxide/boron-doped graphitic carbon nitride composite. *Chem. Eng. J.* **2021**, *403*, 126213. [[CrossRef](#)]
22. Macías-Tamez, R.; Villanueva-Rodríguez, M.; Ramos-Delgado, N.A.; Maya-Treviño, L.; Hernández-Ramírez, A. Comparative Study of the Photocatalytic Degradation of the Herbicide 2,4-D Using  $\text{WO}_3/\text{TiO}_2$  and  $\text{Fe}_2\text{O}_3/\text{TiO}_2$  as Catalysts. *Water Air Soil Pollut.* **2017**, *228*, 379. [[CrossRef](#)]
23. Mugunthan, E.; Saidutta, M.B.; Jagadeeshbabu, P.E. Visible light assisted photocatalytic degradation of diclofenac using  $\text{TiO}_2$ - $\text{WO}_3$  mixed oxide catalysts. *Environ. Nanotechnol. Monit. Manag.* **2018**, *10*, 322–330. [[CrossRef](#)]
24. Cordero-García, A.; Turnes Palomino, G.; Hinojosa-Reyes, L.; Guzmán-Mar, J.L.; Maya-Teviño, L.; Hernández-Ramírez, A. Photocatalytic behaviour of  $\text{WO}_3/\text{TiO}_2$ -N for diclofenac degradation using simulated solar radiation as an activation source. *Environ. Sci. Pollut. Res. Int.* **2017**, *24*, 4613–4624. [[CrossRef](#)]
25. Cordero-García, A.; Guzmán-Mar, J.L.; Hinojosa-Reyes, L.; Ruiz-Ruiz, E.; Hernández-Ramírez, A. Effect of carbon doping on  $\text{WO}_3/\text{TiO}_2$  coupled oxide and its photocatalytic activity on diclofenac degradation. *Ceram. Int.* **2016**, *42*, 9796–9803. [[CrossRef](#)]
26. Dekkouché, S.; Morales-Torres, S.; Ribeiro, A.R.; Faria, J.L.; Fontas, C.; Kebiche-Senhadjji, O.; Silva, A.M.T. In situ growth and crystallization of  $\text{TiO}_2$  on polymeric membranes for the photocatalytic degradation of diclofenac and 17 $\alpha$ -ethinylestradiol. *Chem. Eng. J.* **2022**, *427*, 131476. [[CrossRef](#)]
27. Lara-Pérez, C.; Leyva, E.; Zermeño, B.; Osorio, I.; Montalvo, C.; Moctezuma, E. Photocatalytic degradation of diclofenac sodium salt: Adsorption and reaction kinetic studies. *Environ. Earth Sci.* **2020**, *79*, 277. [[CrossRef](#)]
28. John, D.; Rajalakshmi, A.S.; Lopez, R.M.; Achari, V.S.  $\text{TiO}_2$  reduced graphene oxide nanocomposites for the trace removal of diclofenac. *SN Appl. Sci.* **2018**, *2*, 840. [[CrossRef](#)]
29. Švigelj, Z.; Mandić, V.; Ćurković, L.; Biošić, M.; Žmak, I.; Gaborardi, M. Titania-Coated Alumina Foam Photocatalyst for Memantine Degradation Derived by Replica Method and Sol-Gel Reaction. *Materials* **2020**, *13*, 227. [[CrossRef](#)]
30. Papac, J.; Garcia Ballesteros, S.; Tonkovic, S.; Kovacic, M.; Tomic, A.; Cvetnić, M.; Kušić, H.; Senta, I.; Terzić, S.; Ahel, M.; et al. Degradation of pharmaceutical memantine by photo-based advanced oxidation processes: Kinetics, pathways and environmental aspects. *J. Environ. Chem. Eng.* **2023**, *11*, 109334. [[CrossRef](#)]
31. Li, M.C.; Shen, J.N. Photoelectrochemical oxidation behavior of organic substances on  $\text{TiO}_2$  thin-film electrodes. *J. Solid State Electrochem.* **2006**, *10*, 980–986. [[CrossRef](#)]
32. Kratochvilová, K.; Hoskocová, I.; Jirkovský, J.; Klíma, J.; Ludvík, J. A spectroelectrochemical study of chemisorption, anodic polymerization and degradation of salicylic acid on conductor and  $\text{TiO}_2$  surfaces. *Electrochim. Acta* **1995**, *40*, 2603–2609. [[CrossRef](#)]
33. Zhang, Q.; Zhu, J.; Wang, Y.; Feng, J.; Yan, W.; Xu, H. Electrochemical assisted photocatalytic degradation of salicylic acid with highly ordered  $\text{TiO}_2$  nanotube electrodes. *Appl. Surf. Sci.* **2014**, *308*, 161–169. [[CrossRef](#)]
34. Loukopoulos, S.; Toumazatou, A.; Sakellis, E.; Xenogiannopoulou, V.; Boukos, N.; Dimoulas, A.; Likodimos, V. Heterostructured  $\text{CoO}_x$ - $\text{TiO}_2$  Mesoporous/Photonic Crystal Bilayer Films for Enhanced Visible-Light Harvesting and Photocatalysis. *Materials* **2020**, *13*, 4305. [[CrossRef](#)]
35. Tian, M.; Adams, B.; Wen, J.; Asmussen, R.M.; Chen, A. Photoelectrochemical oxidation of salicylic acid and salicylaldehyde on titanium dioxide nanotube arrays. *Electrochim. Acta* **2009**, *54*, 3799–3805. [[CrossRef](#)]
36. Bhardwaj, S.; Sharma, D.; Kumari, P.; Pal, B. Influence of photodeposition time and loading amount of Ag co-catalyst on growth, distribution and photocatalytic properties of Ag@ $\text{TiO}_2$  nanocatalysts. *Opt. Mater.* **2020**, *106*, 109975. [[CrossRef](#)]
37. Bracco, E.; Butler, M.; Carnelli, P.; Candal, R.  $\text{TiO}_2$  and N- $\text{TiO}_2$ -photocatalytic degradation of salicylic acid in water: Characterization of transformation products by mass spectrometry. *Environ. Sci. Pollut. Res.* **2020**, *27*, 28469–28479. [[CrossRef](#)]
38. Apostolaki, M.-A.; Toumazatou, A.; Antoniadou, M.; Sakellis, E.; Xenogiannopoulou, E.; Gardelis, S.; Boukos, N.; Falaras, P.; Dimoulas, A.; Likodimos, V. Graphene Quantum Dot- $\text{TiO}_2$  Photonic Crystal Films for Photocatalytic Applications. *Nanomaterials* **2020**, *10*, 2566. [[CrossRef](#)]
39. Chachvalvutikul, A.; Luangwanta, T.; Pattison, S.; Hutchings, G.J.; Kaowphong, S. Enhanced photocatalytic degradation of organic pollutants and hydrogen production by a visible light-responsive  $\text{Bi}_2\text{WO}_6/\text{ZnIn}_2\text{S}_4$  heterojunction. *Appl. Surf. Sci.* **2021**, *544*, 148885. [[CrossRef](#)]
40. Božanić, D.K.; Garcia, G.A.; Nahon, L.; Sredojević, D.; Lazić, V.; Vukoje, I.; Ahrenkiel, S.P.; Djoković, V.; Šljivančanin, Ž.; Nedeljkovic, J.M. Interfacial Charge Transfer Transitions in Colloidal  $\text{TiO}_2$  Nanoparticles Functionalized with Salicylic acid and 5-Aminosalicylic acid: A Comparative Photoelectron Spectroscopy and DFT Study. *J. Phys. Chem. C* **2019**, *123*, 29057–29066. [[CrossRef](#)]
41. Roncaroliz, F.; Blesa, M.A. Kinetics of adsorption of carboxylic acids onto titanium dioxide. *Phys. Chem. Chem. Phys.* **2010**, *12*, 9938–9944. [[CrossRef](#)]
42. Tang, W.-R.; Wu, T.; Lin, Y.-W. Salicylic acid-sensitized titanium dioxide for photocatalytic degradation of fast green FCF under visible light irradiation. *Micro Nano Lett.* **2019**, *14*, 359–362. [[CrossRef](#)]
43. Zarei, E. Electrochemically assisted photocatalytic removal of m-cresol using  $\text{TiO}_2$  thin film-modified carbon sheet photoelectrode. *Int. J. Ind. Chem.* **2018**, *9*, 285–294. [[CrossRef](#)]
44. Chatzitakis, A.; Papaderakis, A.; Karanasios, N.; Georgieva, J.; Pavlidou, E.; Litsardakis, G.; Poullos, I.; Sotiropoulos, S. Comparison of the photoelectrochemical performance of particulate and nanotube  $\text{TiO}_2$  photoanodes. *Catal. Today* **2017**, *280*, 14–20. [[CrossRef](#)]

45. Pablos, C.; Marugán, J.; van Grieken, R.; Adán, C.; Riquelme, A.; Palma, J. Correlation between photoelectrochemical behaviour and photoelectrocatalytic activity and scaling-up of P25-TiO<sub>2</sub> electrodes. *Electrochim. Acta* **2014**, *130*, 261–270. [[CrossRef](#)]
46. Teixeira, S.; Martins, P.M.; Lanceros-Méndez, S.; Kühn, K.; Cuniberti, G. Reusability of photocatalytic TiO<sub>2</sub> and ZnO nanoparticles immobilized in poly(vinylidene difluoride)-co-trifluoroethylene. *Appl. Surf. Sci.* **2016**, *384*, 497–504. [[CrossRef](#)]
47. Gerischer, H. The impact of semiconductors on the concepts of electrochemistry. *Electrochim. Acta* **1990**, *35*, 1677–1699. [[CrossRef](#)]
48. Matarrese, R.; Mascia, M.; Vacca, A.; Mais, L.; Usai, E.M.; Ghidelli, M.; Mascaretti, L.; Bricchi, B.R.; Russo, V.; Casari, C.S.; et al. Integrated Au/TiO<sub>2</sub> Nanostructured Photoanodes for Photoelectrochemical Organics Degradation. *Catalysts* **2019**, *9*, 340. [[CrossRef](#)]
49. Colucci, J.; Montalvo, V.; Hernandez, R.; Pouillet, C. Electrochemical oxidation potential of photocatalyst reducing agents. *Electrochim. Acta* **1990**, *44*, 2507–2514. [[CrossRef](#)]
50. Zrinski, I.; Martinez, S.; Gospić, E. A catalytic and photocatalytic effects of TiO<sub>2</sub> nanoparticles on electrooxidation of common antioxidants on carbon past. *J. Solid State Electrochem.* **2021**, *25*, 1591–1600. [[CrossRef](#)]
51. Fischer, K.; Sydow, S.; Griebel, J.; Naumov, S.; Elsner, C.; Thomas, I.; Abdul Latif, A.; Schulze, A. Enhanced Removal and Toxicity Decline of Diclofenac by Combining UVA Treatment and Adsorption of Photoproducts to Polyvinylidene Difluoride. *Polymers* **2020**, *12*, 2340. [[CrossRef](#)]
52. Zhang, Z.; Yuan, Y.; Fang, Y.; Liang, L.; Ding, H.; Shi, G.; Jin, L. Photoelectrochemical oxidation behavior of methanol on highly ordered TiO<sub>2</sub> nanotube array electrodes. *J. Electroanal. Chem.* **2007**, *610*, 179–185. [[CrossRef](#)]
53. Radić, G.; Šajnović, I.; Petrović, Ž.; Kraljić Roković, M. Reduced Graphene Oxide/ $\alpha$ -Fe<sub>2</sub>O<sub>3</sub> Fibres as Active Material for Supercapacitor Application. *Croat. Chem. Acta* **2018**, *91*, 481–490. [[CrossRef](#)]
54. Hankin, A.; Bedoya-Lora, F.E.; Alexander, J.C.; Regoutz, A.; Kelsall, G.H. Flat band potential determination: Avoiding the pitfalls. *J. Mater. Chem. A* **2019**, *7*, 26162–26176. [[CrossRef](#)]
55. Kovacic, M.; Kusic, H.; Fanetti, M.; Lavrencic Stangar, U.; Valant, M.; Dionysios, D.D.; Loncaric Bozic, A. TiO<sub>2</sub>-SnS<sub>2</sub> nanocomposites: Solaractive photocatalytic materials for water. *Environ. Sci. Pollut. Res.* **2017**, *24*, 19965–19979. [[CrossRef](#)]
56. Sharifi, T.; Crmaric, D.; Kovacic, M.; Kraljic Rokovic, M.; Kusic, H.; Jozic, D.; Ambrozic, G.; Kralj, D.; Kontrec, J.; Zener, B.; et al. Tailored BiVO<sub>4</sub> for enhanced visible-light photocatalytic performance. *J. Environ. Chem. Eng.* **2021**, *9*, 106025. [[CrossRef](#)]
57. Mu, J.; Miao, H.; Liu, E.; Feng, J.; Teng, F.; Zhang, D.; Kou, Y.; Jin, Y.; Fan, J.; Hu, X. Enhanced light trapping and high charge transmission capacities of novel structures for efficient photoelectrochemical water splitting. *Nanoscale* **2018**, *10*, 11881–11893. [[CrossRef](#)]
58. Zhang, Y.C.; Li, J.; Xu, H.Y. One-step in situ solvothermal synthesis of SnS<sub>2</sub>/TiO<sub>2</sub> nanocomposites with high performance in visible light-driven photocatalytic reduction of aqueous Cr(VI). *Appl. Catal. B* **2012**, *123–124*, 18–26. [[CrossRef](#)]
59. Frisch, M.J.; Trucks, G.W.; Schlegel, H.B.; Scuseria, G.E.; Robb, M.A.; Cheeseman, J.R.; Scalmani, G.; Barone, V.; Petersson, G.A.; Nakatsuji, H.; et al. *Gaussian 16, Revision C.01*; Gaussian, Inc.: Wallingford, CT, USA, 2016.
60. Becke, A.D. Density-functional thermochemistry. III. The role of exact exchange. *J. Chem. Phys.* **1993**, *98*, 5648–5652. [[CrossRef](#)]
61. Lee, C.; Yang, W.; Parr, R.G. Development of the Colle-Salvetti correlation-energy formula into a functional of the electron density. *Phys. Rev. B* **1998**, *37*, 785–789. [[CrossRef](#)]
62. Vosko, S.H.; Wilk, L.; Nusair, M. Accurate spin-dependent electron liquid correlation energies for the local spin density calculations: A critical analysis. *Can. J. Phys.* **1980**, *58*, 1200–1211. [[CrossRef](#)]
63. Stephens, P.J.; Devlin, F.J.; Chabalowski, C.F.; Frisch, M.J. Ab initio calculation of vibrational absorption and circular dichroism spectra using density functional force field. *J. Phys. Chem.* **1994**, *98*, 11623–11627. [[CrossRef](#)]
64. Krishnan, R.; Binkley, J.S.; Seeger, R.; Pople, J.A. Self-consistent molecular orbital methods. XX. A basis set for correlated wave functions. *J. Chem. Phys.* **1980**, *72*, 650–654. [[CrossRef](#)]
65. Cossi, M.; Barone, V.; Cammi, R.; Tomasi, J. Ab initio study of solvated molecules: A new implementation of the polarizable continuum model. *Chem. Phys. Lett.* **1996**, *255*, 327–335. [[CrossRef](#)]
66. Lipparini, F.; Scalmani, G.; Mennucci, B.; Cances, E.; Caricato, M.; Frisch, M.J. A variational formulation of the polarizable continuum model. *J. Chem. Phys.* **2010**, *133*, 014106. [[CrossRef](#)] [[PubMed](#)]

**Disclaimer/Publisher's Note:** The statements, opinions and data contained in all publications are solely those of the individual author(s) and contributor(s) and not of MDPI and/or the editor(s). MDPI and/or the editor(s) disclaim responsibility for any injury to people or property resulting from any ideas, methods, instructions or products referred to in the content.